Acoustic metamaterial capsule for reduction of stage machinery noise

Anton Melnikov, Marcus Maeder, Niklas Friedrich, Yan Pozhanka, Alexander Wollmann, Michael Scheffler, Sebastian Oberst, David Powell, and Steffen Marburg

Citation: The Journal of the Acoustical Society of America **147**, 1491 (2020); doi: 10.1121/10.0000857
View online: https://doi.org/10.1121/10.0000857
View Table of Contents: https://asa.scitation.org/toc/jas/147/3
Published by the Acoustical Society of America

JASA ARTICLE

Acoustic metamaterial capsule for reduction of stage machinery noise

Anton Melnikov,[1,a)] Marcus Maeder,[1] Niklas Friedrich,[2] Yan Pozhanka,[3] Alexander Wollmann,[4] Michael Scheffler,[4] Sebastian Oberst,[5] David Powell,[6] and Steffen Marburg[1]

[1]*Chair of Vibroacoustics of Vehicles and Machines, Boltzmannstrasse 15, Technical University of Munich, Garching, Bavaria 85748, Germany*

[2]*SBS Bühnentechnik GmbH, Bosewitzer Strasse 20, Dresden, Saxony 01259, Germany*

[3]*CADFEM-CIS, Kondrat'yevskiy Prospekt 15, Saint Petersburg, Northwestern Federal District 195197, Russia*

[4]*Applied Mechanics Group, University of Applied Sciences, Kornmarkt 1, Zwickau, Saxony 08056, Germany*

[5]*Centre for Audio, Acoustics and Vibration University of Technology Sydney, 15 Broadway, Sydney, New South Wales 2007, Australia*

[6]*School of Engineering and Information Technology, University of New South Wales, Northcott Drive, Canberra, Australian Capital Territory 2612, Australia*

ABSTRACT:

Noise mitigation of stage machinery can be quite demanding and requires innovative solutions. In this work, an acoustic metamaterial capsule is proposed to reduce the noise emission of several stage machinery drive trains, while still allowing the ventilation required for cooling. The metamaterial capsule consists of c-shape meta-atoms, which have a simple structure that facilitates manufacturing. Two different metamaterial capsules are designed, simulated, manufactured, and experimentally validated that utilize an ultra-sparse and air-permeable reflective meta-grating. Both designs demonstrate transmission loss peaks that effectively suppress gear mesh noise or other narrow band noise sources. The ventilation by natural convection was numerically verified, and was shown to give adequate cooling, whereas a conventional sound capsule would lead to overheating. The noise spectra of three common stage machinery drive trains are numerically modelled, enabling one to design meta-gratings and determine their noise suppression performance. The results fulfill the stringent stage machinery noise limits, highlighting the benefit of using metamaterial capsules of simple c-shape structure. https://doi.org/10.1121/10.0000857

(Received 25 September 2019; revised 28 January 2020; accepted 19 February 2020; published online 5 March 2020)

[Editor: Kai Ming Li] Pages: 1491–1503

I. INTRODUCTION

Noise control in mechanical and civil engineering requires compact, efficient, and low maintenance solutions. In particular, the control of noise emitted by machinery operating in theaters or operas, such as stage elevator drive trains, is quite demanding, with the emission limits being as close as possible to that of the background noise levels.[1–3] This is naturally challenging for stage machinery designers, especially when the constraints of the venue do not allow the application of conventional noise control measures, such as elastic bearings, noise barriers, or sound capsules. Noise at frequencies below 1000 Hz is especially problematic, since conventional noise insulation structures are quite bulky at these frequencies, and space is generally a scarce resource in a stage environment.

One of the main noise sources of stage machinery drive trains are the gear boxes, where the noise is dominated by the gear mesh frequencies and their higher harmonics.[4–6] Figure 1 shows a measured noise spectrum of a typical stage machinery gearbox, showing a small number of distinct peaks. The strongest peak is found below 1000 Hz, and its suppression would be the most effective means to reduce the overall noise emission. Since the stage machinery manufacturer is unable to influence the noise emission of the gearboxes directly, secondary noise control measures are required. Sound capsules can be very effective for noise reduction, but also have drawbacks, which limit their applicability to stage machinery. First, sound capsules are often ineffective below 1000 Hz, which is often the most important frequency range, and second, typical sound capsules do not allow air flow, which may lead to overheating of the encapsulated machinery. Typically, stage machinery is operated in intermittent periodic duty cycle S3 40%, which requires sufficient heat exchange by forced or natural convection.[7] Therefore, in this work a novel meta-capsule (acoustic metamaterial capsule) is introduced, which can overcome these drawbacks.

Acoustic metamaterials offer a broad variety of opportunities to manipulate propagating acoustic waves[8] by

[a)]Also at: SBS Bühnentechnik GmbH, Bosewitzer Strasse 20, Dresden, Saxony 01259, Germany. Electronic mail: anton.melnikov@tum.de

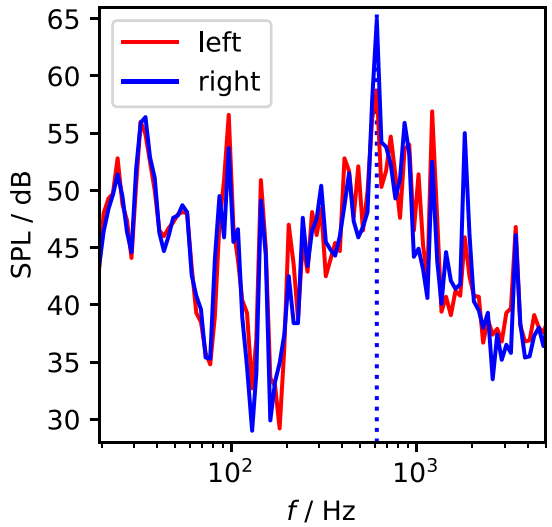

FIG. 1. (Color online) Noise emission of a gearbox of a rope drive system for left and right rotation directions as by the gear box supplier. The blue dotted vertical indicates the frequency of the highest emission.

introducing media properties such as negative bulk modulus[9] or negative dynamic mass density.[10] These principles have been utilized to create acoustic superlenses[11–13] and acoustic barriers.[14–16] The latter is a promising approach for noise control, where useful concepts have already been demonstrated.[17–21]

Fard *et al.*[17] conducted a numerical study on periodic Helmholtz resonators showing promising results for noise control applications over a frequency range of more than one octave. Henneberg *et al.*[18] demonstrated and experimentally verified an elastic stop-band material to reduce velocity cross-coupling of ultrasonic transducers by 10 dB. In a subsequent study, Henneberg *et al.*[19] expanded the ideas to multi-frequency applications. Claeys *et al.*[20] presented a sound insulating meta-capsule comprised of elastic resonators embedded in a two-dimensional lattice, reducing sound pressure level (SPL) by 20 dB. Marinova *et al.*[21] realised a transmission loss of up to 25 dB at 130 Hz for a membrane-type metamaterial noise barrier. However, these approaches all make use of an airtight sound capsule, preventing ventilation and increasing the risk of machinery overheating.

Metamaterials which allow air flow have been developed, based on perforated membranes[22,23] and space coiling structures.[24–28] The air-permeable meta-grating realized by Cheng *et al.*[24] demonstrated 93% insertion loss while having a thickness 0.15 times the wavelength at 500 Hz. Later, a whole acoustic metacage allowing forced fluid flow through it was designed and verified experimentally by Shen *et al.*[29] All of these approaches rely on reflection or redirection of the sound wave, without attempting to engineer absorption. Acoustic metamaterial absorbers have been proposed.[30–33] Wu *et al.*[30] make use of energy dissipation due to the friction in thin channels during the resonance. This principle allows an absorption of 88.9% to be achieved with a single layer of metamaterial.[31] Lee *et al.*[32] proposed arrays of paired Helmholtz resonators with an absorption of over 90% at 2200 Hz that could simultaneously be used to control the direction of air flow. Xiang *et al.*[33] designed a stackable, ultra-open metamaterial absorber with broadband performance, having a measured absorption coefficient above 0.6 for a frequency range between 500 and 720 Hz. Although many acoustic metamaterials have been developed and experimentally verified, there have been very few demonstrations of their performance outside of a controlled laboratory environment. Acoustic metamaterials which allow for ventilation have been applied to windows,[34,35] where the noise spectra and suppression requirements differ significantly from those of machinery noise.[1,3,36]

An important drawback of the structures presented in Refs. 23, 24, and 32 is that they strongly reflect the incident field only within a narrow frequency range. This can limit the noise control applications of acoustic metamaterials to tasks where the noise emission is dominated by narrow band peaks. Gear boxes are generally known to produce narrow band noise spectra,[4–6] where a measurement example of gear induced SPL with a narrow peak is shown in Fig. 1. Accordingly, effective noise reduction of such emissions by a narrow band meta-grating is possible, but only if the meta-grating is tailored to the noise spectrum of the source. To date, it has not been demonstrated whether acoustic metamaterial sound barriers allowing ventilation can meet the requirements for machinery noise control.

The desired properties of metamaterials originate from localized resonances, asymmetries, or phase shifts in periodically arranged unit cells, called meta-atoms. The design of such properties requires complex fine features or exotic geometric shapes, which usually require sophisticated manufacturing technologies. However, the resonant properties required for strong reflection can be achieved with simpler meta-atom structures. Recently, we demonstrated a c-shape meta-atom consisting of a cylindrical Helmholtz resonator,[37] which facilitates manufacturing using conventional industrial technologies, e.g., mechanical processing. Furthermore, this meta-atom provides a number of additional properties such as reduced thermo-viscous losses and coupling between the monopolar and dipolar degrees of freedom, known as Willis coupling,[38] which gives additional flexibility in controlling the acoustic response of a metamaterial. It was demonstrated that Willis coupling can be tailored to achieve any value up to the theoretical limit.[37,39] The ease of manufacturing the metamaterial structures presented in Ref. 37 makes them an ideal building block for air-permeable noise control structures, building on the concepts presented in Refs. 24 and 32.

In this work we present a metamaterial capsule design and apply it directly to stage machinery in order to reduce the noise induced by gears. In Sec. II, we design a reflective meta-grating based on c-shape meta-atoms and, subsequently, we expand this design to a full 3D meta-capsule prototype. The transmission loss of this prototype is modelled numerically and verified experimentally. In Sec. III, a meta-capsule is designed for the rope drive system, one of the most common drive trains in stage machinery. The transmission loss of the meta-grating is tailored to the measured noise spectrum of the gear-box. The numerically determined

https://doi.org/10.1121/10.0000857

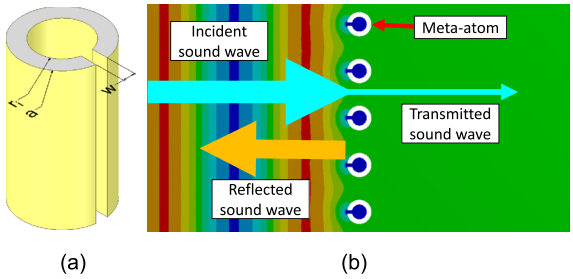

FIG. 2. (Color online) (a) c-shape meta-atom with dimensions, as proposed in Ref. 37. (b) FEM simulation of wave reflection from the meta-grating. The background color scheme shows the magnitude of the sound pressure.

transmission loss is then compared with the measurements under realistic conditions. Furthermore, the ventilation performance of the meta-capsule is verified by numerical studies considering natural convection. In Sec. IV, we demonstrate a numerical approach for modelling of stage machinery noise induced by gearboxes. It is applied to three typical stage machinery drive trains: push chain, gear rack, and spiralift. We then identify critical emission peaks of these drive trains and propose tailored multilayer meta-gratings for effective noise reduction while still allowing ventilation.

II. META-CAPSULE PROTOTYPE

Inspired by the promising concepts proposed by Quan *et al.*,[39] Cheng *et al.*,[24] and Lee *et al.*[32] we use a resonant c-shape meta-atom[37] to create a 2D meta-grating. The c-shape meta-atom is shown in Fig. 2(a) and has the following dimensions: outer radius $a = 19\,\text{mm}$, inner radius $r_i = 12\,\text{mm}$, and neck width $w = 5.5\,\text{mm}$. Positioning the meta-atoms periodically with a lattice constant (distance between the meta-atoms) of $d = 4a = 76\,\text{mm}$ creates a meta-grating, as shown in Fig. 2(b). Due to the strong response of the meta-atoms, this meta-grating can significantly affect the sound field and provide strong reflection of the acoustic waves even when the meta-atoms are arranged to have notable gaps between them.

The transmission loss of the meta-grating was calculated by the finite element method (FEM) using ANSYS MULTIPHYSICS[40] for a normally incident wave. The mesh element size was 1 mm inside and around the meta-atom, while the size in all other regions was 3 mm. The element type is a 20-node element with a quadratic interpolation function. The transmission loss is calculated without considering impedance boundary conditions or thermo-viscous losses, and it is shown in Fig. 3(a) (red solid line) with a peak of 97 dB located at 1513 Hz. This transmission loss was achieved for a 2D geometry, with no obliquely incident wave components, so it neglects several important 3D effects which can reduce the transmission loss.

To expand the 2D meta-surface to a 3D structure, we design a meta-capsule prototype to reduce emission from the encapsulated noise source to the outside of the meta-capsule. The meta-capsule is a box with dimensions 350 mm × 310 mm × 310 mm and its structure and photograph are shown in Figs. 3(b) and 3(c), respectively. The role of the meta-grating is to reflect acoustic waves and any

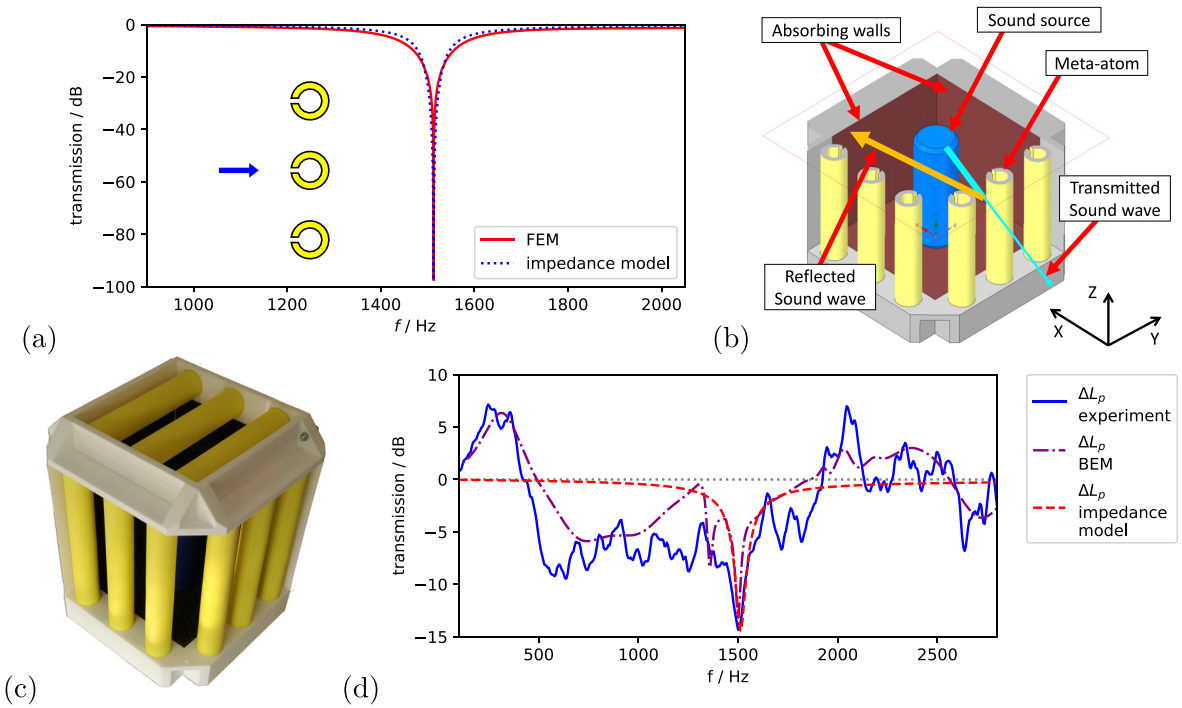

FIG. 3. (Color online) (a) Transmission loss determined using FEM (red solid line) and impedance model [blue dotted line, according to Eq. (3)] for a normally incident wave (blue arrow) for infinite meta-grating with a lattice constant $d = 76\,\text{mm}$. (b) Meta-capsule prototype concept: the sound wave is redirected by the meta-grating to the absorbing wall. (c) Photograph of manufactured meta-capsule. (d) Transmission of the meta-capsule prototype measured (blue solid line) and simulated (purple dash-dotted line). Red dashed line shows transmission of the meta-capsule calculated using Eq. (3). ΔL_p is the ratio between the sound radiation with and without the meta-capsule.

internal losses within the c-shaped elements will cause unwanted transmission of waves. Therefore, we separate the absorption and reflection functions into different walls of the meta-capsule. Three sides of the meta-capsule contain an air-permeable meta-grating to redirect the sound wave and the side opposite each meta-grating contains absorbing foam to dissipate the redirected wave. Figure 3(b) shows a schematic of the incident wave generated by the sound source being reflected by the meta-grating and subsequently being absorbed by the foam.

To determine the transfer function of the 3D meta-capsule prototype, we apply the in-house 3D boundary element method (BEM) code AKUSTA, using continuous elements with a quadratic interpolation function.[41–43] The sound source was modelled as a chamfered cylinder, matching the shape of the commercial loudspeaker model *Ultimate Ears Boom 2*, with a diameter of 65 mm and height of 180 mm. This loudspeaker is used subsequently for the experimental validation. A normal surface velocity of 1 m/s was applied uniformly over the source surface. The acoustic transfer function was determined by analyzing two situations, a free loudspeaker on the bottom plate and a loudspeaker covered by the meta-capsule. The sound pressure was compared at the reference point $\mathbf{r}_{\text{ref}} = [-1, 0, 0]$ m relative to the center of the source, as per the coordinate system shown in Fig. 3(b). The density and acoustic velocity of air were set to $\rho_0 = 1.2\,\text{kg}\,\text{m}^{-3}$ and $c = 343\,\text{m}\,\text{s}^{-1}$, respectively.

Figure 3(d) shows the simulated transmission of the capsule at the reference point $\mathbf{r}_{\text{ref}}$ (purple dash-dotted line). A transmission loss peak of 13 dB is observed at 1500 Hz, corresponding to the transmission loss peak of the 2D meta-surface. The curve demonstrates additional features, including a valley between 500 and 1300 Hz with a transmission loss of up to 6 dB and a smaller peak of 8 dB at 1350 Hz. Additionally, an increase in transmission is present below 500 Hz with a peak of 7 dB at 300 Hz and above 2000 Hz with values up to 3 dB. So long as this transmission increase does not correspond to any of the noise peaks of the encapsulated machinery, it will have minimal effect on the total noise emission. However, the drop of 13 dB at the operating frequency of 1500 Hz shows that the meta-capsule is promising for the suppression of narrowband noise sources.

While the transmission loss at 1500 Hz can be readily explained by the transmission properties of the 2D meta-grating, to understand the other features, we need to consider the change in power radiated by the loudspeaker when the meta-capsule is added (see blue solid line with stars in Fig. 4). It is observed that the radiated source power depends on the frequency, and it is suppressed in regions between 600 and 1300 Hz and 1550 and 1800 Hz. Consequently, this changes the SPL measured outside the meta-capsule, where a similar reduction is present (see red dashed line in Fig. 4). Therefore, the broadband transmission effects observed in the SPL are mainly due to the change of the source's radiation impedance. This same effect is responsible for the increase in emission below 500 Hz and above 1800 Hz, where the meta-capsule effectively becomes an impedance-matching structure. Similarly, the farfield radiated power (see dark-blue solid line with crosses in Fig. 4) follows the trend of the source radiated power, however, the farfield power has a negative peak close to 1500 Hz caused by the meta-grating. The change of the source radiated power is linked to the Purcell effect in optics,[44] which was recently demonstrated experimentally for acoustic waves.[45,46] Related discussions of the influence of radiation impedance on the radiated sound power can be found in several textbooks.[47,48]

A. Experimental validation of the prototype

For experimental validation of the acoustic transfer function, the meta-capsule prototype was manufactured. The individual parts were printed using selective laser sintering from polyamide and mounted together using silicone to seal the gaps. The absorbing walls were created by gluing a 40 mm layer of the commercial absorbing material *Cellofoam 471/SK*[49] onto a 10 mm layer of polyamide. The

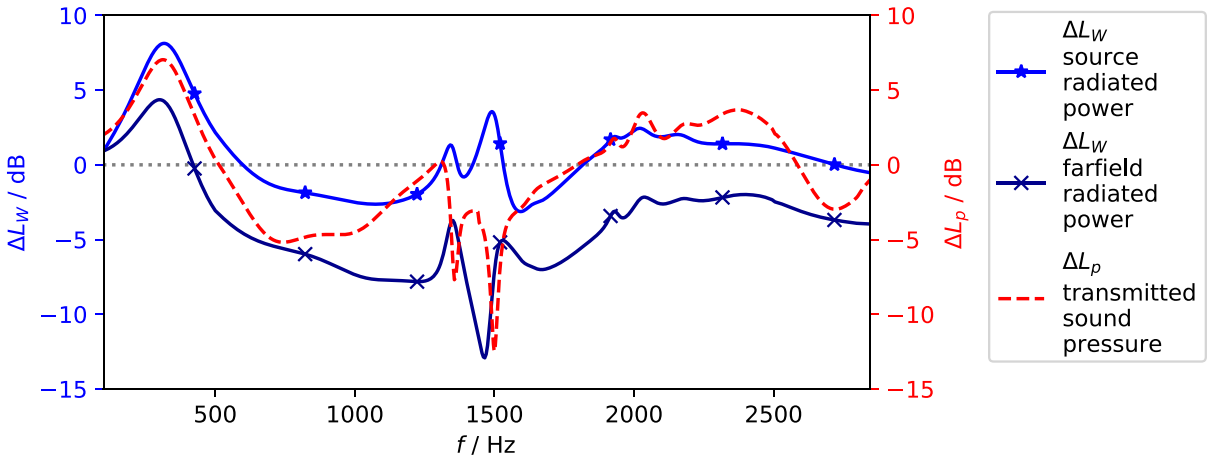

FIG. 4. (Color online) Numerically calculated change in sound power radiated from the loudspeaker and farfield radiated power, compared with the sound pressure transmitted through the meta-capsule prototype shown in Fig. 3(b). Broadband regions of SPL attenuation are caused by the change of the radiated source power, due to the change of the radiation impedance induced by the meta-capsule.

https://doi.org/10.1121/10.0000857

transfer function was determined using white noise excitation of the loudspeaker and recording the sound pressure with a Bruel&Kjaer hand-held analyzer type 2270, equipped with an 1/2-in free-field microphone type 4189 and a ZC-0032 preamplifier. The microphone was calibrated before measurement with the pistonphone type 4228 (Bruel&Kjaer), and the calibration was verified after measurement to ensure parameters had not changed during measured. The measurement was executed in an environment with a background noise level at least 10 dB below the measured values in the frequency range of interest. The microphone was positioned at the same reference point as in numerical simulation, $\mathbf{r}_{\mathrm{ref}} = [-1, 0, 0]$ m. The transmission loss was determined by comparing measured sound pressure with and without the meta-capsule.

The measured transmission function of the manufactured meta-capsule prototype is shown as the blue solid line in Fig. 3(d). The maximum transmission loss at 1500 Hz is about 14 dB, which is slightly above the numerically predicted value of 13 dB. This peak is caused by the meta-grating. Over the frequency range between 500 and 2000 Hz, the transmission is reduced by approximately 7 dB, similar to the numerical result. Furthermore, we can observe an increase in transmission below 500 Hz and above 1800 Hz, due to the change in radiation impedance of the source.

B. Transmission loss modeling using impedance

The transmission loss peak of the meta-capsule can be calculated using a simple impedance model for acoustic filters.[48,50] From the response shown in Supplementary Equation S37 of Ref. 37 we can write the impedance of a layer of meta-atoms as

$$Z_{\mathrm{MA}}(\omega) = \frac{2A_d}{A_w}\left(i\omega\rho_0 l_{\mathrm{eff}} + b - \frac{i}{\omega}\frac{K}{V}A_w\right), \tag{1}$$

where A_d is the meta-grating cross section belonging to one meta-atom, A_w is the c-shape's aperture cross section, i is the imaginary unit, ω is the angular frequency, ρ_0 is the density of air, $l_{\mathrm{eff}} = l + c_{\mathrm{eff}}w$ is the effective aperture length,[48] K is the bulk modulus of air, V is the c-shape's inner volume, and b is the damping. Considering the characteristic impedance of air $Z_0 = \rho_0 c$, we can write the impedance of the meta-grating as

$$Z_{\mathrm{MG}} = \left(\frac{1}{Z_{\mathrm{MA}}} + \frac{1}{Z_0}\right)^{-1}. \tag{2}$$

Subsequently, the transmission can be calculated according to

$$\Delta L_p = 20\log_{10}\left(1 - \left|\frac{Z_{\mathrm{MG}} - Z_0}{Z_{\mathrm{MG}} + Z_0}\right|\right). \tag{3}$$

Figure 3(a) demonstrates how this model matches the numerical results for a plane wave incident upon an infinite meta-grating. The empirical parameters $c_{\mathrm{eff}} = 1.6$ and $b = 1 \times 10^{-4}$ Pa s m^{-1} were found to produce good agreement. Furthermore, Eq. (3) can be used to predict the transmission peak of the meta-capsule. However, due to finite meta-grating size and oblique incidence angle the transmission loss peak observed in Fig. 3(d) is less effective. Subsequently, to represent the efficiency drop the damping can be set to an artificial value $b = 1.75$ Pa s m^{-1}, which results in good agreement with simulation and experiment [see Fig. 3(d), red dashed line]. In Sec. IV we consider multilayer meta-gratings, where N different meta-atom layers of multilayer meta-grating can be combined as

$$Z_{\mathrm{MG}} = \left(\sum_{n=1}^{N}\frac{1}{Z_{\mathrm{MA},n}} + \frac{1}{Z_0}\right)^{-1}. \tag{4}$$

III. DESIGN AND EXPERIMENTAL VALIDATION IN APPLICATION

A. Design for a rope drive system

Rope drives are very popular for applications with high acoustic requirements, since they allow a very quiet stage machinery to be constructed.[51] Although many other noise sources are avoided in rope drive systems, gearboxes are still required and their noise emission can be highly intrusive when not masked by additional noise sources. The rope drive system considered herein is shown in Fig. 5(a). The electric motor drives a pair of rope drums using silent chains. The measured noise emission of the gear box used for this system is presented in Fig. 1 for both rotation directions. It was observed that a dominant peak is present at 613 Hz (blue dotted vertical line), which is especially prominent for the right rotation. Therefore, in the following we propose a tailored meta-capsule to reduce this peak.

For this purpose we designed a meta-grating, which provides maximum transmission loss at 613 Hz. The meta-atom uses the c-shape presented in Fig. 2(a) with different dimensions: outer radius $a = 42.5$ mm, inner radius $r_i = 32.5$ mm, neck width $w = 10.6$ mm, and lattice constant $d = 110$ mm. The photograph of the designed and manufactured meta-capsule is shown in Fig. 5(b). The meta-grating is placed at one side of the capsule only and its surface normal is aligned parallel with the motor shaft. It has size 590 mm × 530 mm and consists of an array of five meta-atoms. The meta-atoms are made from polyamide using selective laser sintering. To suppress vertical modes inside the c-shape cavity, two metal sheets divide the meta-grating into three regions. The central field has a missing meta-atom in the center to provide clearance necessary for the connection of the emergency drive. All other walls of the meta-capsule are made of steel sheets of thickness 2 mm combined with commercial absorber *Cellofoam 471/SK*[49] of thickness 40 mm. The meta-capsule encapsulates only the electric motor and the gear-box. The air flow necessary for ventilation is only possible through the meta-grating.

Based on the new geometry, the meta-grating transmission can be estimated with the red dashed curve in Fig. 5(c) according to Eq. (3). Using $b = 1.5$ Pa s m^{-1} results in 17 dB

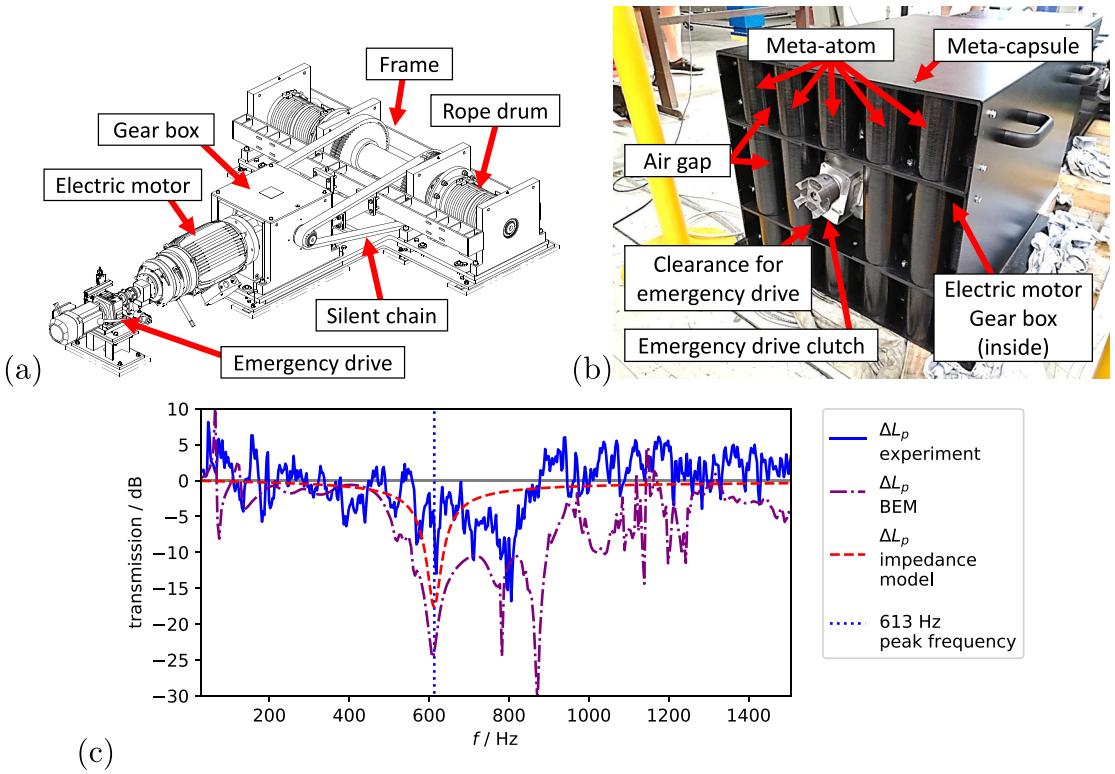

FIG. 5. (Color online) (a) Rope drive system with labels. (b) Photograph of the meta-capsule with electric motor and gear box inside. (c) Measured (blue solid line), simulated (purple dash-dotted line), and empirically estimated [Eqs. (3), red dashed line] transmission profile of the meta-capsule. Vertical blue dotted line corresponds to the peak observed in Fig. 1. ΔL_p is the ratio between the sound radiation with and without the meta-capsule.

transmission loss, which is close to the results demonstrated for the prototype meta-capsule in Fig. 3(d). Furthermore, we determine the transfer function of the meta-capsule by means of 3D BEM using continuous elements with a quadratic interpolation function. For simplification, the motor and the gearbox have been assumed to be the only sound sources in the model. The normal surface velocity was normalized to $v_n = 1\,\mathrm{m\,s^{-1}}$ and applied uniformly over the motor and gear box surfaces. The sound transfer function was determined by calculating transmitted pressure for the electric motor and gear box inside the meta-capsule, and normalising this to pressure for the same situation with the meta-grating removed on one side only. The medium density and the speed of sound are set to $\rho_0 = 1.2\,\mathrm{kg\,m^{-3}}$ and $c = 343\,\mathrm{m\,s^{-1}}$, respectively. The numerically determined transmission profile is shown by the purple dash-dotted line in Fig. 5(c). Three transmission loss peaks are observed, 24 dB at 613 Hz, 24 dB at 780 Hz, and 30 dB at 880 Hz. The peak at 613 Hz is caused by the tailored meta-grating design.

B. Experimental validation in application

The designed meta-capsule was manufactured using the procedure outlined in Sec. II A. For the absorbing walls, the porous material was attached to 2 mm thick steel sheets. The meta-capsule's transfer function was determined using the natural excitation of all active components during the operation at maximum rotational speed of approximately $1490\,\mathrm{min^{-1}}$. The data was acquired with a 1/4-in free-field PCB microphone and Squadriga Frontend (Head Acoustics). The microphone was calibrated with a pistonphone type 4230 B&K (Bruel&Kjaer). The measurements were conducted in a factory building, with a background noise level of at least 10 dB below the measured values in the frequency range of interest. The microphone position was 1 m away from the meta-grating and was concentric with the motor shaft axis. The transmission loss was determined the same way as for the prototype meta-capsule.

The measured transmission is shown in Fig. 5(c). The measurement confirms a peak very close to 613 Hz with a transmission loss of 14 dB. The measured transmission loss at the peak is less than that prediction by numerical calculation and closer to the value predicted by Eq. (3). We note that the meta-grating thickness is 85 mm, which is 0.15λ at 613 Hz (λ is the wavelength) hence below $\lambda/4$. There are two additional peaks present in the measurement, around 700 Hz and around 800 Hz. The confirmation of the designed transmission loss peak demonstrates the feasibility of the meta-capsule concept in application.

C. Ventilation performance of the meta-capsule

To demonstrate the ventilation properties of the designed meta-capsule, we conducted 3D Computational Fluid Dynamics (CFD) simulations solving the non-linear Navier-Stokes equations with the commercial code ANSYS FLUENT.[40] This allows the steady-state temperature during

https://doi.org/10.1121/10.0000857

operation to be determined, considering natural convection, and determining heat dissipation from the efficiency of the drive unit. The electric motor has a nominal power of 27 kW, which already includes a margin of safety $S = 2$ required by the DIN 56950-1:2012-05 stage machinery standard.[52] The used efficiency factors are $\eta = 0.94$ for the motor and $\eta = 0.97$ for the gear box, resulting in heating powers of 810 and 381 W, respectively. The periodic duty of the stage machinery is usually defined as S3 40%,[7] which means an operation duration of maximum 40% during a 10 min cycle. For steady state configuration, this periodic duty type reduces the heating power by a factor of 0.4. For turbulent regions of air flow induced by natural convection we applied the k-ω SST turbulence model[53,54] with the constants $\alpha_{\text{inf}} = 1$, $\alpha^*_{\text{inf}} = 0.52$, $\beta^*_{\text{inf}} = 0.09$, $a_1 = 0.31$, $\beta_i^{\text{Inner}} = 0.075$, and $\beta_i^{\text{Outer}} = 0.0828$. The environmental temperature was 20 °C. The heat transfer coefficient of the acoustic absorber was considered as $h_{\text{Cello}} = 0.04\,\text{W m}^{-1}\,\text{K}^{-1}$ as specified by the manufacturer.[49]

The CFD results at steady state are shown in Fig. 6. In Fig. 6(a) we observe that the meta-grating allows sufficient cooling by natural convection. It leads to a motor surface temperature of 85 °C, which is within the bounds given in Table VII of Ref. 7. However, as shown in Fig. 6(b), a conventional air-tight sound capsule would lead to temperatures above 140 °C, which would cause overheating of the electric motor (see Table VII in Ref. 7). Following this, a conventional sound capsule would not be recommended to be used in combination with the simulated drive train.

IV. MODELLING OF STAGE MACHINERY NOISE

In this section, we numerically analyze the application of the meta-capsule to the suppression of noise in other types of stage machinery, namely, push chain, gear rack, and spiralift systems. To design the meta-capsules, it is necessary to first characterize the noise emission from these stage machinery systems. All three systems had been designed to reduce the noise emission by the empirical methods common in stage machinery.

In this work we consider only the gear induced excitation, since this typically dominates stage machinery noise. The analysis of vibration due to mechanical motion was done with the FEM, using the commercial software package ANSYS.[40] To determine the excitation forces, the gear mesh process was modelled for each system using FEM. The material of the gears and shafts is steel, with a Young's modulus of $E_{\text{St}} = 200$ GPa, a Poisson ratio of $\nu_{\text{St}} = 0.3$, and a density of $\rho_{\text{St}} = 7850\,\text{kg m}^{-3}$. The fluctuation of the meshing force, which is affected by the time-varying mesh stiffness, is known to be the major source of noise and vibration.[5,6] We use this force fluctuation to model the source in our analysis. As demonstrated in Refs. 5 and 6, the normal modes of the gears and the shafts can be neglected for the determination of the dynamic bearing force. Under the assumption of periodic excitation forces, the loads are transferred to the frequency domain with harmonic time dependence. This allows subsequent analysis of steady-state time-harmonic dynamics by means of the harmonic response.

The harmonic response was calculated using full powertrain models up to 2500 Hz utilizing a modal superposition procedure with a preceding modal analysis up to 5000 Hz. The frequency range was limited by the model dimensions of several meters [see Figs. 8(a), 9(a), and 10(a)] but is sufficient to cover the important noise frequency range of stage machinery. Due to the complexity of the real structure and lack of accurate data, a representative damping ratio of $\xi = 3 \times 10^{-2}$ was considered, as is commonly recommended for metal structures with joints.[55] The harmonic analysis yields the surface velocities of the whole structure required for the subsequent acoustic analysis.

At low frequencies, the directivity of the sound can be neglected, which allows the full acoustic analysis to be reduced to a sound power analysis. The calculation of the sound power of a mechanical system is usually done by solving a Robin problem with known normal velocity, known admittance boundary condition, and unknown sound pressure. After the sound pressure is obtained, the sound power follows as[56,57]

$$P = \frac{1}{2}\Re\left\{\int_\Gamma p(x) v_n^*(x)\,\mathrm{d}\Gamma\right\}, \tag{5}$$

where $p(x)$ is sound pressure, $v_n^*(x)$ is the complex conjugate of the normal surface velocity of the fluid, and Γ is fluid-structure interface.

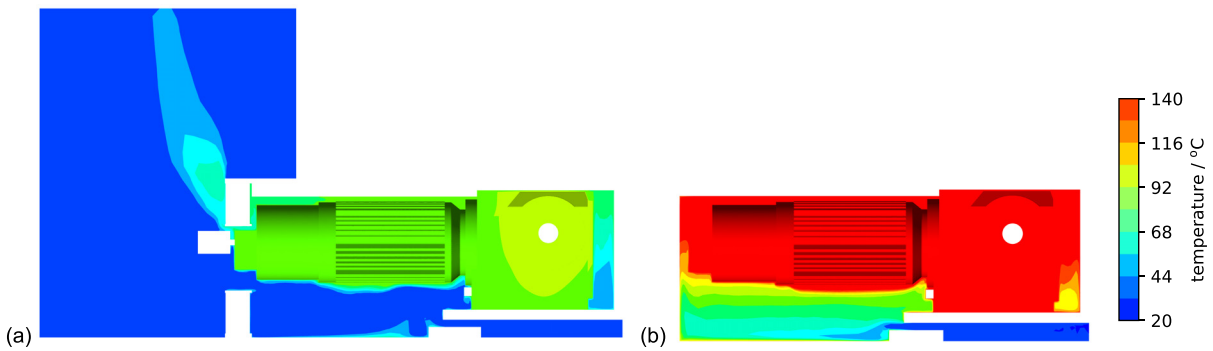

FIG. 6. (Color online) Temperature profile due to natural convection during stationary operation of the motor covered by (a) an air-permeable meta-capsule and (b) an airtight conventional sound capsule calculated using CFD. The meta-capsule results in a temperature of ≈85 °C at the motor surface, whereas a conventional sound capsule would cause overheating of the motor with temperatures >140 °C.

If large models have to be considered, computation of sound pressure p requires significant computational effort, which can imply restrictions for geometrical details and for the frequency range. The computation of sound pressure can be avoided by utilizing sound power approximation methods, such as equivalent radiated power (ERP) or the lumped parameter model (LPM).[56,58,59] ERP uses the assumption of unit radiation efficiency for the whole fluid-structure interface. Therefore, application of ERP on the power trains typically overestimates the sound power in the lower frequency range.[59] The LPM avoids general overestimation at low frequencies and is able to consider acoustic short circuits. This method is based on the approximation of the Rayleigh integral and is written as[56,59]

$$P_{\mathrm{LPM}} = \frac{1}{2} k\rho c \sum_{\mu} \sum_{\nu} \frac{\sin\left(k|\mathbf{r}_\mu - \mathbf{r}_\nu|\right)}{2\pi|\mathbf{r}_\mu - \mathbf{r}_\nu|} \Re\{v_\mu v_\nu^*\} A_\mu A_\nu. \tag{6}$$

More details on the performance of these methods can be found in Refs. 59, 60.

Commonly, the noise limits in stage machinery address the middle of the first row of the auditorium, see Fig. 7. To study the SPL at this location geometrical acoustics was solved using COMSOL MULTIPHYSICS.[61] Therefore, this study considers only the air transmission path between the location of the drive train and the middle of the first row. The effective distance and the absorption of the surfaces are different in every venue, therefore the sound transfer function strongly depends on the hall. To determine the transfer function, a geometrical model of the auditorium including the stage is required. The newly build venue *Kraftwerk Mitte* in Dresden (Germany) was chosen as a reference hall for modeling of the transfer function. Thus, a model was derived from the geometry of the venue *Kraftwerk Mitte*. The absorption coefficients of the walls and chairs were updated to represent the measured reverberation times. Additionally, the transmission loss of the stage floor separating the drive train location from the stage area was determined experimentally and implemented in the model. Finally, this model was used to determine the SPL in the middle of first row of auditoria originating from LPM sound power of two machines of the same kind below the stage (see Fig. 7).

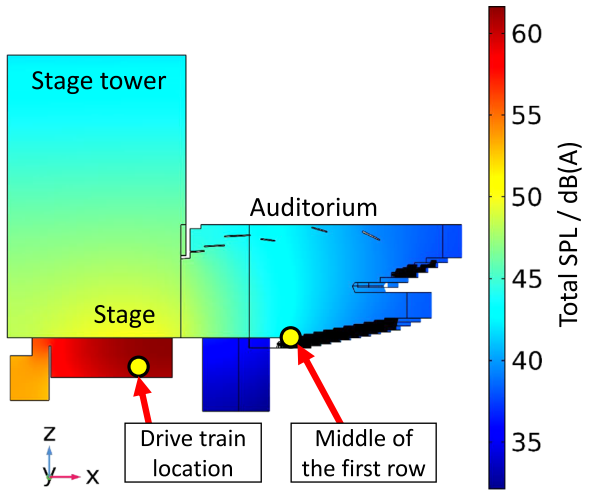

FIG. 7. (Color online) Sound level distribution calculated by geometrical acoustics in *Kraftwerk Mitte* (Dresden). The important locations are that of the drive trains below the stage and the reference point in the middle of the first row.

Recently, we analyzed SPL data in the middle of the first row taken during live performances and proposed five different limit curves: opera standard, opera sensitive, ballet standard, ballet sensitive, and drama.[3] These performance curves are illustrated in Figs. 8(c), 9(c), and 10(c). To avoid disturbance of the audience during the performance, stage machinery noise emission should remain below these limits. The simulation produces discrete frequency spectra, whereas the SPL limits are defined in octave bands.[3] The measured SPL results from analog filtering of the sound analyzer. This filtering was reproduced by a digital Butterworth filter applied to the simulation data to enable its comparison with the limits obtained from analog measurements.[3]

Here, we present the numerical results of stage machinery noise. We observe that the considered noise spectra are dominated by a few sharp peaks, which can be reduced by surrounding the machinery in a meta-capsule. Furthermore, based on the previously presented outcomes, we propose a multi-layer meta-grating to reduce the noise emission during scenic performance to allowable levels.

A. Push chain

The FEM model of the push chain system demonstrating a vibration mode at 273 Hz is shown in Fig. 8(a). The simulated SPL in the first row is illustrated in Fig. 8(b) as a narrow-band spectrum (cyan solid line) and in Fig. 8(c) in octaves (red solid line with crosses). Furthermore, Fig. 8(c) shows five different noise limits in the first row of the auditorium during a scenic performance (dark lines with smaller markers).[3] Comparison of the noise emission with the noise limits in Fig. 8(c) reveals that the emission exceeds some limits at 250 Hz, 1 kHz, and 2 kHz octaves.

Analyzing the noise spectrum in Fig. 8(b) allows the identification of critical peaks at 273, 1367, and 1638 Hz (cyan solid line). These peaks dominate the octave levels exceeding the limits. The critical peaks can be reduced by combining three different meta-gratings in a multilayer metamaterial. To match the peak frequencies with the transmission loss peaks the meta-grating should consist of the following c-shape geometries (a, l, w) in mm: (82, 10, 10), (20, 5.2, 6), and (16, 4, 4). The lattice constant was set to $d = 4a$ for all geometries. The empirical damping used in Eq. (3) was interpolated, then extrapolated as

$$b(f) = b_1 + \frac{b_2 - b_1}{f_2 - f_1}(f - f_1), \tag{7}$$

where f is the frequency, $b_1 = 1.5\,\mathrm{Pa\,s\,m^{-1}}$, $f_1 = 613\,\mathrm{Hz}$, $b_2 = 1.75\,\mathrm{Pa\,s\,m^{-1}}$, and $f_2 = 1500\,\mathrm{Hz}$ according to Secs. II and III. Using Eqs. (3) and (4), the transmission of such

https://doi.org/10.1121/10.0000857

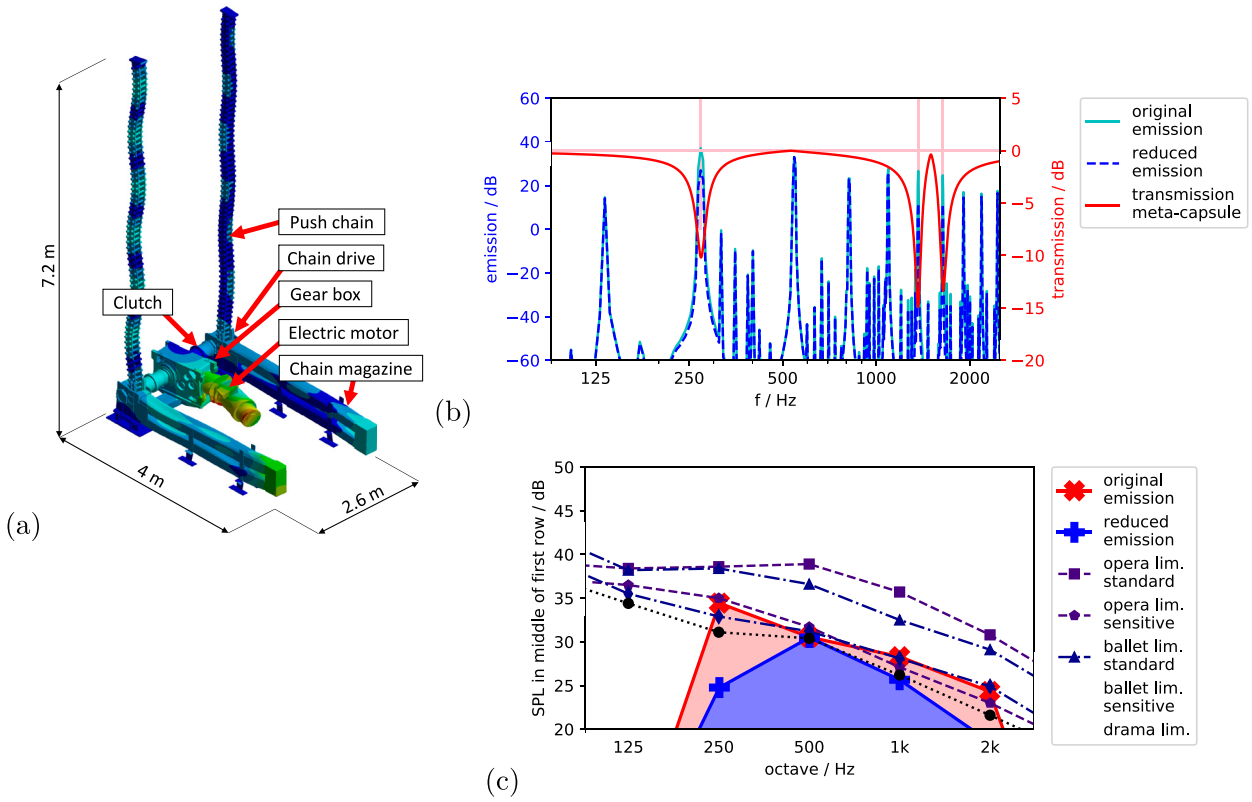

FIG. 8. (Color online) (a) Components and dimensions of the push chain system. The plot reveals a vibration mode at 273 Hz. (b) Simulated emission of the push chain system (cyan solid line) and the reduced emission by meta-capsule design (blue dashed line). The transmission of the meta-capsule (red solid line) is based on Eqs. (3) and (4) and tailored for the three critical emission peaks. (c) Original and reduced noise emission compared with the stage machinery noise limits in octaves.

multilayer metamaterial can be estimated by the red solid line shown in Fig. 8(b). Application of this transmission on the noise spectrum leads to the blue dashed line in Fig. 8(b), where the identified peaks are significantly reduced compared to the original emission (cyan solid line). The reduced emission in octaves is shown in Fig. 8(c), where now all five limit types are fulfilled at 250 Hz and 2 kHz. At the 500 Hz and 1 kHz octave bands, the sensitive limits for opera and ballet are fulfilled as well, whereas the drama limit (black dotted line with circles) is still slightly exceeded by approximately 1 dB.

B. Gear rack

The gear rack system is shown in Fig. 9(a). It illustrates a vibration mode at 545 Hz. Figure 9(b) illustrates the narrow-band SPL in the middle of the first row as a cyan solid line. Figure 9(c) shows the SPL in the middle of the first row in octaves (red solid line with crosses). It is observed in Fig. 9(b) that the sensitive limits are strongly violated for the 1 kHz octave band. Additionally, drama and sensitive ballet limits are slightly exceeded at the 2 kHz octave band.

The limit violation can be traced back to the SPL peaks at 817.0, 1094.2, and 1638.7 Hz [see Fig. 9(b)]. Based on these peaks the required c-shape geometries were chosen for (a, l, w) in mm: (32, 7, 8.5), (24, 6, 6), (16, 4, 4) with $d = 4a$ and b according to Eq. (7). The transmission function of such multilayer metamaterials is estimated using Eqs. (3) and (4) and is depicted by the red solid line in Fig. 9(b). Application of these transfer functions on the noise emission leads to reduced emission shown in Fig. 9(b) (blue dashed line) and in Fig. 9(c) (blue solid line with pluses). It can be observed that all limits are fulfilled in Fig. 9(c).

C. Spiralift system

Figure 10(a) shows the spiralift system. This system differs slightly from the push chain and gear rack because it has two chains that require a chain tightener. The chain tightener provides local modes with relatively low eigenfrequencies. These modes get excited and even if the chain tightener area is relatively small, the magnitudes are large enough to produce dominant noise peaks. Such a mode at 282 Hz is illustrated in Fig. 10(a) producing the strongest SPL peak in Fig. 10(b) (cyan solid line). The resulting octave levels are demonstrated in Fig. 10(c) (red solid line with crosses), where almost all limits are violated between the 250 Hz and 2 kHz octave bands.

Since there are four octaves where the emission has to be reduced, at least four peaks are to be treated, one per octave. This requires a multilayer metamaterial with four different meta-grating layers. The critical peaks occur at 282, 560, 1119, and 1678 Hz in Fig. 10. The required c-shape geometries (a, l, w) in mm were chosen as (80, 9, 10), (45, 9.5, 10), (24, 7, 6), (16, 4, 4.5) with $d = 4a$ and b according to Eq. (7). The transmission function of the

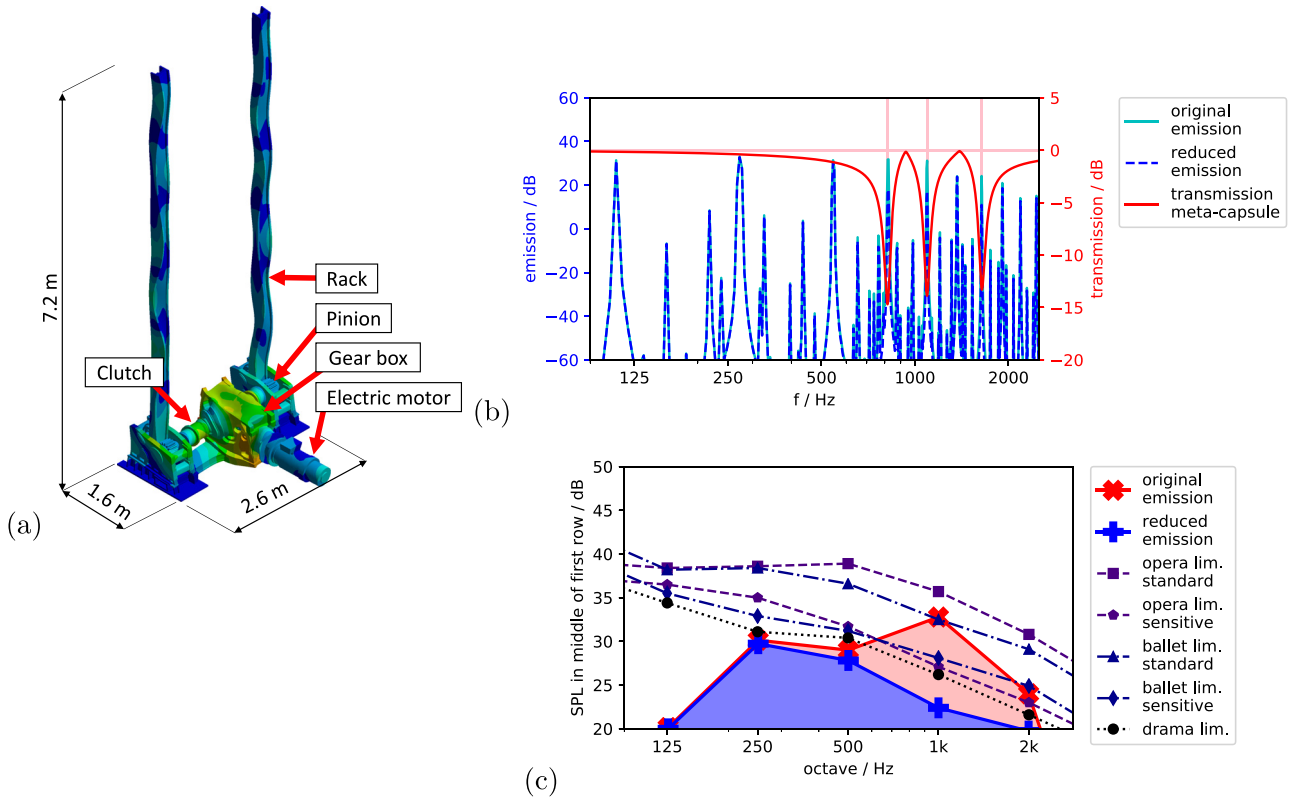

FIG. 9. (Color online) (a) Components and dimensions of the gear rack system. The plot reveals a vibration mode at 545 Hz. (b) Simulated emission of the gear rack system (cyan solid line) and the reduced emission by meta-capsule design (blue dashed line). The transmission of the meta-capsule (red solid line) is based on Eqs. (3) and (4) and tailored for the three critical emission peaks. (c) Original and reduced noise emission compared with the stage machinery noise limits in octaves.

metamaterial was estimated using Eqs. (3) and (4) and is shown in Fig. 10(b) as the red solid line. The reduced emission is shown in Fig. 10(b) as the blue dashed line and in Fig. 10(c) in octaves (blue solid line with pluses). The reduced emission fulfills standard opera and standard ballet limits. Furthermore, all limits are fulfilled for the 250 Hz octave band, whereas sensitive opera, sensitive ballet, and drama limits are still exceeded by up to 5 dB.

V. DISCUSSION

Two meta-capsules were investigated experimentally and numerically. In the case of the meta-capsule prototype, a reasonable agreement between simulation and experiment was demonstrated, see Fig. 3(d). The same level of agreement could not be observed during the validation of the meta-capsule on the rope drive system [see Fig. 5(c)], nevertheless, the existence of the transmission loss peak caused by the meta-grating was confirmed. The deviations can be attributed to geometrical simplification during the BEM modelling, misalignment during the manufacturing of the capsule, and neglect of the sound radiation contribution from the outer meta-capsule surfaces. Due to the simple geometry of the meta-capsule prototype, we were able to represent its shape exactly in the simulation. However, in the case of the rope drive system, the complex geometry of the cooling ribs of the electric motor [see Fig. 5(a)] and some additional details had to be simplified before BEM modelling. Furthermore, sometimes the absorbing foam could not be mounted as intended during the design, which reduced the capsule's inner volume. The volume reduction could explain the shift of the peak pair from around 700 and 800 Hz in the experiment to around 780 and 880 Hz in the simulation. Finally, the BEM model considers only the noise radiated by the surface of the electric motor and the gear box, whereas many more surfaces contribute to the total sound radiation. We note that under these imperfect but realistic conditions, a transmission loss was still observed.

We demonstrated the potential of noise emission reduction based on three common stage machinery systems. In all three cases we could identify and treat the critical peaks in a way that the noise limits could be fully or partially fulfilled. Complete numerical modelling was not feasible due to the large model size compared to the required details of the metamaterial. Therefore, the transmission loss was estimated by the impedance model in Eqs. (3) and (4). This approach gives the engineer a simple tool for designing such meta-gratings, as was demonstrated for these three examples. Additionally, the cooling performance of the multilayer meta-gratings can be tailored using CFD to fulfill the allowable temperatures similarly to the single-layer meta-grating shown in Sec. III C.

An alternative noise control solution allowing ventilation can be realized using sonic crystals.[15] We therefore

https://doi.org/10.1121/10.0000857

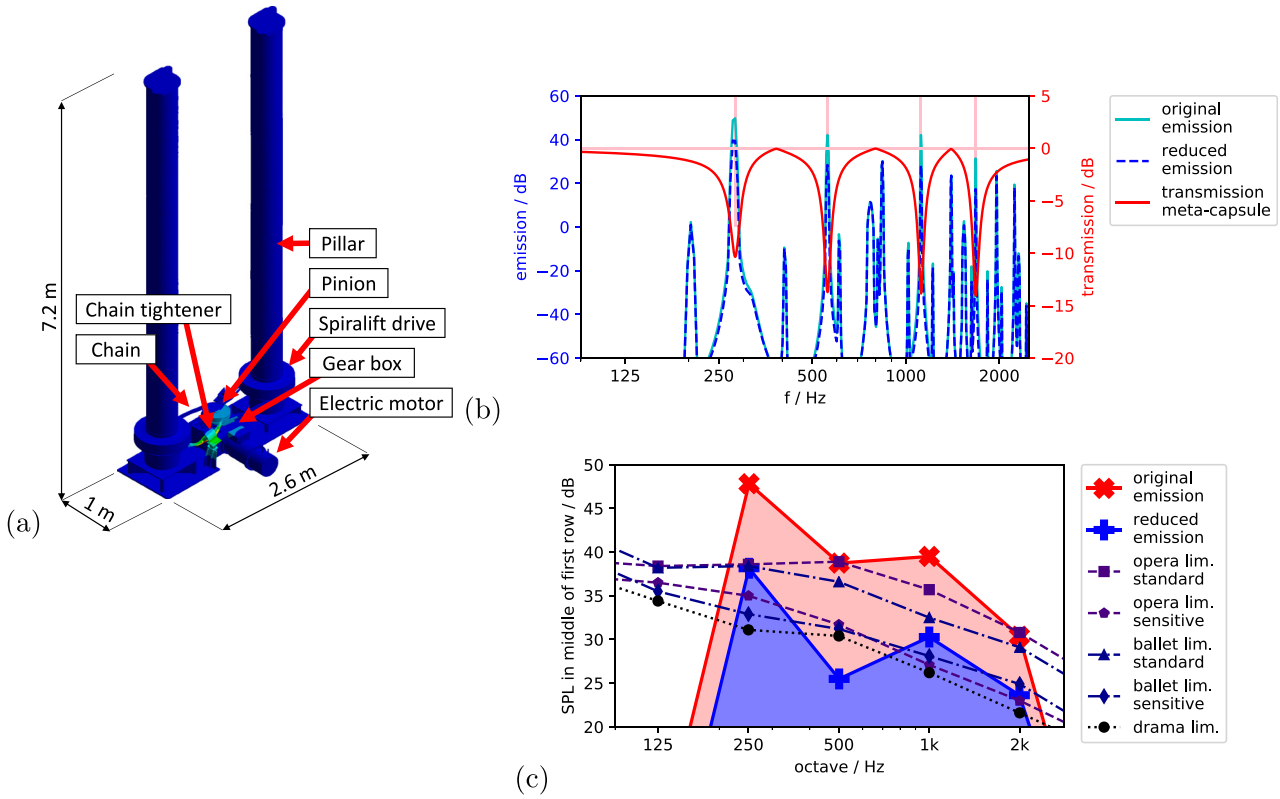

FIG. 10. (Color online) (a) Components and dimensions of the spiralift system. The plot reveals a local vibration mode at 282 Hz. (b) Simulated emission of the spiralift system (cyan solid line) and the reduced emission by meta-capsule design (blue dashed line). The transmission of the meta-capsule (red solid line) is based on Eqs. (3) and (4) and tailored for the four critical emission peaks. (c) Original and reduced noise emission compared with the stage machinery noise limits in octaves.

benchmark our meta-grating against a sonic crystal consisting of meta-atoms outlined in Sec. II. We also compare the performance of rigid cylinders in meta-grating and sonic crystal configurations, with a radius similar to that of the meta-atom radius a. The lattice constant used for sonic crystals is $d = 4a$. In Fig. 11, the c-shape sonic crystal demonstrates two band gaps in the considered frequency range: 1333 to 1591 Hz and 1980 to 2636 Hz, where the first band gap is linked to the meta-atom resonance. Considering the sonic crystal of cylinders leads to only one band gap between 1744 and 2606 Hz. The effect of the band gaps can be observed in the transmission loss of the sonic crystal

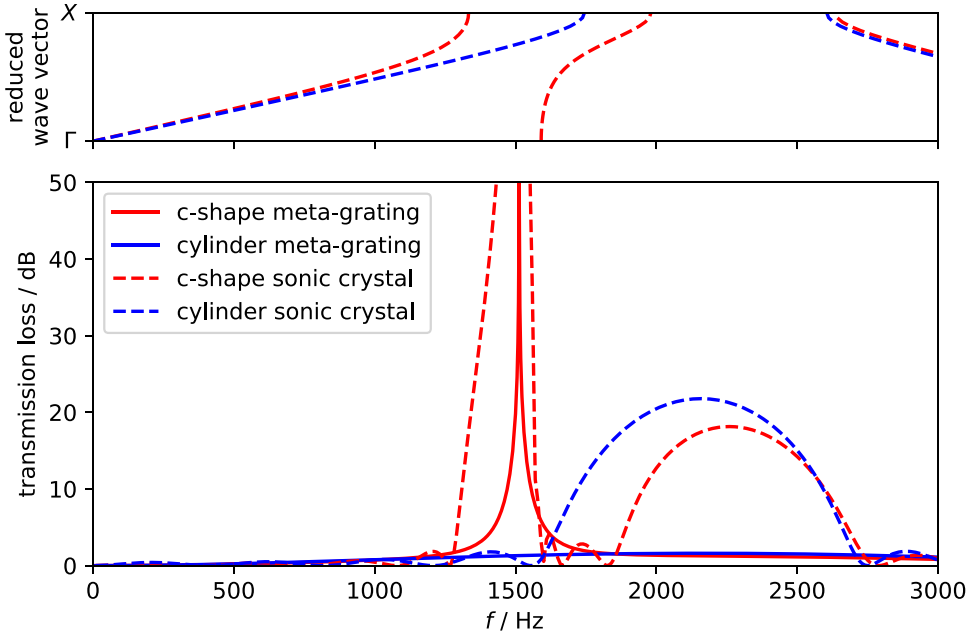

FIG. 11. (Color online) Dispersion relation for c-shape and cylinder sonic crystals and comparison of transmission loss for four different cases: c-shape meta-grating, cylinder meta-grating, c-shape sonic crystal with five unit cells, and cylinder sonic crystal with five unit cells.

(dashed curves), where the first band gap of the c-shape sonic crystal causes large transmission loss. Comparing that with the c-shape meta-grating reveals that the sonic crystal reflects the sound over a broader frequency range. However, the price for better performance is a thickness of five unit cells being $(5+4)2a$, which equals approximately 1.5λ at 1500 Hz. The increased thickness makes the sonic crystal less attractive for applications which have limited space, including stage machinery.

We note that the designed meta-gratings are ultra-sparse, having a thickness much smaller than the wavelength at the frequency of the maximum transmission loss. The meta-grating designed for the meta-capsule prototype with $a = 19$ mm is 0.17λ, while the meta-grating designed for the rope drive system with $a = 42.5$ mm reaches 0.15λ. The latter value is similar to the factor achieved by Cheng *et al.*[24] and demonstrates the effectiveness of the c-shape meta-atom. Furthermore, we observe in Fig. 11 that the sonic crystal of cylinders reveals a transmission loss up to 20 dB in the band gap, whereas the meta-grating of cylinders is not able to provide any noticeable transmission loss in the considered frequency range. This indicates that the transmission loss of the c-shape meta-grating is primarily due to local resonances of each meta-atom, rather than Bragg reflection between multiple meta-atoms.

VI. CONCLUSION

In this study, we investigated the reduction of noise emission from stage machinery using c-shape meta-atoms, with simple geometry that facilitates relatively easy manufacturing. We designed a 2D meta-grating and expanded it to a 3D meta-capsule prototype, which we investigated experimentally and numerically. In both experiment and simulation, a significant transmission drop at the resonant frequency of the meta-grating was observed. Furthermore, additional attenuation was present over a broad frequency range around the operating frequency, in addition to the narrow band attenuation of the meta-grating. Subsequently, this concept was verified by designing and manufacturing a meta-capsule for a rope drive system common in stage machinery. A transmission loss peak at resonant frequency could be observed experimentally. Additionally, it was numerically proven that the meta-capsule provides sufficient ventilation for cooling of the motor by natural convection. Finally, we modelled the noise of three other drive train types typically used in stage machinery, where a violation of stage machinery noise limits in the first row of the auditorium was present. Identification of critical peaks and subsequent design of tailored meta-gratings was demonstrated to reduce the noise emission. Following this, the presented concept provides a new horizon for noise control in stage machinery and other noise sensitive branches. This work demonstrates benefits and limitations of acoustic meta-capsules for noise control applications. To an engineer, it offers a simple concept for using acoustic meta-materials in daily work.

ACKNOWLEDGMENTS

A.M., M.M., N.F., M.S., and S.M. acknowledge funding supported by the German Federal Ministry for Economic Affairs and Energy under the index ZF4128201AT5. The authors acknowledge Yan Kei Chiang from UNSW Canberra for useful discussions on impedance modelling.

[1]L. L. Beranek, "Revised criteria for noise in buildings," Noise Control **3**(1), 19–27 (1957).
[2]H.-P. Tennhardt, "Grenzwerte der schallimmission buehnentechnischer anlagen" ["Limits for noise immission of stage machinery installations"], IEMB Infoblaetter **5**, 1–4 (1998).
[3]A. Melnikov, I. Witew, M. Maeder, M. Gatt, M. Scheffler, and S. Marburg, "Sound pressure level limits for stage machinery noise in operas and theaters," Appl. Acoust. **156**, 29–39 (2019).
[4]A. Melnikov, M. Scheffler, and S. Marburg, "Untersuchungen eines Bühnenpodiums hinsichtlich der Reduktion von Geräuschemission" ["Investigations of a stage elevator concerning noise reduction"], *Proceedings of DAGA2017 Kiel* (2017).
[5]R. Müller, "Schwingungs- und Geräuschanregung bei Stirnradgetrieben" ["Vibration and noise of spur gears"] (1991).
[6]J. Zhou and S. Wenlei, "Vibration and noise radiation characteristics of gear transmission system," J. Low Freq. Noise Vib. Active Control **33**(4), 485–502 (2014).
[7]IEC 60034-1:2010: "Rotating electrical machines—Part 1: Rating and performance" (2010).
[8]S. A. Cummer, J. Christensen, and A. Alù, "Controlling sound with acoustic metamaterials," Nat. Rev. Mater. **1**(3), 16001 (2016).
[9]N. Fang, D. Xi, J. Xu, M. Ambati, W. Srituravanich, C. Sun, and X. Zhang, "Ultrasonic metamaterials with negative modulus," Nat. Mater. **5**(6), 452–456 (2006).
[10]Z. Liu, X. Zhang, Y. Mao, Y. Y. Zhu, Z. Yang, C. T. Chan, and P. Sheng, "Locally resonant sonic materials," Science **289**(5485), 1734–1736 (2000).
[11]M. Ambati, N. Fang, C. Sun, and X. Zhang, "Surface resonant states and superlensing in acoustic metamaterials," Phys. Rev. B **75**(19), 195447 (2007).
[12]S. Zhang, L. Yin, and N. Fang, "Focusing ultrasound with an acoustic metamaterial network," Phys. Rev. Lett. **102**(19), 194301 (2009).
[13]D. Torrent and J. Sánchez-Dehesa, "Acoustic metamaterials for new two-dimensional sonic devices," New J. Phys. **9**(9), 323 (2007).
[14]J. V. Sánchez-Pérez, D. Caballero, R. Mártinez-Sala, C. Rubio, J. Sánchez-Dehesa, F. Meseguer, J. Llinares, and F. Gálvez, "Sound attenuation by a two-dimensional array of rigid cylinders," Phys. Rev. Lett. **80**(24), 5325–5328 (1998).
[15]D. P. Elford, L. Chalmers, F. V. Kusmartsev, and G. M. Swallowe, "Matryoshka locally resonant sonic crystal," J. Acoust. Soc. Am. **130**(5), 2746–2755 (2011).
[16]F. Langfeldt, W. Gleine, and O. von Estorff, "Analytical model for low-frequency transmission loss calculation of membranes loaded with arbitrarily shaped masses," J. Sound Vib. **349**, 315–329 (2015).
[17]S. M. B. Fard, H. Peters, S. Marburg, and N. Kessissoglou, "Acoustic performance of a barrier embedded with Helmholtz resonators using a quasi-periodic boundary element technique" (2017).
[18]J. Henneberg, A. Gerlach, H. Storck, H. Cebulla, and S. Marburg, "Reducing mechanical cross-coupling in phased array transducers using stop band material as backing," J. Sound Vib. **424**, 352–364 (2018).
[19]J. Henneberg, A. Gerlach, H. Cebulla, and S. Marburg, "The potential of stop band material in multi-frequency ultrasonic transducers," J. Sound Vib. **452**, 132–146 (2019).
[20]C. Claeys, E. Deckers, B. Pluymers, and W. Desmet, "A lightweight vibro-acoustic metamaterial demonstrator: Numerical and experimental investigation," Mech. Syst. Sign. Process. **70-71**, 853–880 (2016).
[21]P. Marinova, S. Lippert, and O. von Estorff, "On the numerical investigation of sound transmission through double-walled structures with membrane-type acoustic metamaterials," J. Acoust. Soc. Am. **142**(4), 2400–2406 (2017).

[22]G. Ma, M. Yang, Z. Yang, and P. Sheng, "Low-frequency narrow-band acoustic filter with large orifice," Appl. Phys. Lett. **103**(1), 011903 (2013).
[23]F. Langfeldt, H. Kemsies, W. Gleine, and O. von Estorff, "Perforated membrane-type acoustic metamaterials," Phys. Lett. A **381**(16), 1457–1462 (2017).
[24]Y. Cheng, C. Zhou, B. G. Yuan, D. J. Wu, Q. Wei, and X. J. Liu, "Ultra-sparse metasurface for high reflection of low-frequency sound based on artificial MIE resonances," Nat. Mater. **14**(10), 1013–1019 (2015).
[25]Z. Chen, L. Fan, S.-y. Zhang, H. Zhang, X.-j. Li, and J. Ding, "An open-structure sound insulator against low-frequency and wide-band acoustic waves," Appl. Phys. Exp. **8**(10), 107301 (2015).
[26]H.-l. Zhang, Y.-f. Zhu, B. Liang, J. Yang, J. Yang, and J.-c. Cheng, "Omnidirectional ventilated acoustic barrier," Appl. Phys. Lett. **111**(20), 203502 (2017).
[27]R. Ghaffarivardavagh, J. Nikolajczyk, S. Anderson, and X. Zhang, "Ultra-open acoustic metamaterial silencer based on Fano-like interference," Phys. Rev. B **99**(2), 024302 (2019).
[28]X. Yu, Z. Lu, T. Liu, L. Cheng, J. Zhu, and F. Cui, "Sound transmission through a periodic acoustic metamaterial grating," J. Sound Vib. **449**, 140–156 (2019).
[29]C. Shen, Y. Xie, J. Li, S. A. Cummer, and Y. Jing, "Acoustic metacages for sound shielding with steady air flow," J. Appl. Phys. **123**(12), 124501 (2018).
[30]X. Wu, C. Fu, X. Li, Y. Meng, Y. Gao, J. Tian, L. Wang, Y. Huang, Z. Yang, and W. Wen, "Low-frequency tunable acoustic absorber based on split tube resonators," Appl. Phys. Lett. **109**(4), 043501 (2016).
[31]X. Wu, K. Y. Au-Yeung, X. Li, R. C. Roberts, J. Tian, C. Hu, Y. Huang, S. Wang, Z. Yang, and W. Wen, "High-efficiency ventilated metamaterial absorber at low frequency," Appl. Phys. Lett. **112**(10), 103505 (2018).
[32]T. Lee, T. Nomura, E. M. Dede, and H. Iizuka, "Ultrasparse acoustic absorbers enabling fluid flow and visible-light controls," Phys. Rev. Appl. **11**(2), 024022 (2019).
[33]X. Xiang, X. Wu, X. Li, P. Wu, H. He, Q. Mu, S. Wang, Y. Huang, and W. Wen, "Ultra-open high-efficiency ventilated metamaterial absorbers with customized broadband performance," arXiv:1911.05969 (2019).
[34]S.-H. Kim and S.-H. Lee, "Air transparent soundproof window," AIP Adv. **4**(11), 117123 (2019).
[35]Y. Ge, H.-x. Sun, S.-q. Yuan, and Y. Lai, "Switchable omnidirectional acoustic insulation through open window structures with ultrathin meta-surfaces," Phys. Rev. Mater. **3**(6), 065203 (2019).
[36]L. L. Beranek, "Balanced noisecriterion (NCB) curves," J. Acoust. Soc. Am. **86**(2), 650–664 (1989).
[37]A. Melnikov, Y. K. Chiang, L. Quan, S. Oberst, A. Alù, S. Marburg, and D. Powell, "Acoustic meta-atom with experimentally verified maximum Willis coupling," Nat. Commun. **10**(1), 3148 (2019).
[38]J. R. Willis, "Effective constitutive relations for waves in composites and metamaterials," Proc. R. Soc. London A: Math. Phys. Eng. Sci. **467**(2131), 1865–1879 (2011).
[39]L. Quan, Y. Radi, D. L. Sounas, and A. Alù, "Maximum Willis coupling in acoustic scatterers," Phys. Rev. Lett. **120**(25), 254301 (2018).
[40]*ANSYS Multiphysics*, Release 19.2, Help System, ANSYS Inc., www.ansys.com (Last viewed 02/29/2020).
[41]S. Marburg and S. Schneider, "Influence of element types on numeric error for acoustic boundary elements," J. Comput. Acoust. **11**(3), 363–386 (2003).
[42]S. Marburg, "The Burton and Miller method: Unlocking another mystery of its coupling parameter," J. Comput. Acoust. **24**(1), 1550016 (2015).
[43]S. Marburg, *Boundary Element Method for Time-Harmonic Acoustic Problems* (Springer, Cham, 2018).
[44]K. H. Drexhage, "Influence of a dielectric interface on fluorescence decay time," J. Lumin. **1-2**, 693–701 (1970).
[45]L. Langguth, R. Fleury, A. Alù, and A. F. Koenderink, "Drexhage's experiment for sound," Phys. Rev. Lett. **116**(22), 224301 (2016).
[46]M. Landi, J. Zhao, W. E. Prather, Y. Wu, and L. Zhang, "Acoustic Purcell effect for enhanced emission," Phys. Rev. Lett. **120**(11), 114301 (2018).
[47]P. M. Morse and K. U. Ingard, *Theoretical Acoustics* (Princeton University Press, Princeton, 1986).
[48]L. E. Kinsler, *Fundamentals of Acoustics* (Wiley, New York, 2000).
[49]"Cellofoam 471 data sheet," https://www.cellofoam.co.uk/fileadmin/user_upload/Data_sheets_English/471_E.pdf (Last viewed 02/29/2020).
[50]K. T. Chen, Y. H. Chen, K. Y. Lin, and C. C. Weng, "The improvement on the transmission loss of a duct by adding Helmholtz resonators," Appl. Acoust. **54**(1), 71–82 (1998).
[51]R. Harris, "The drama of the silent move: Control of noise from stage machinery in the Operaen Copenhagen," Proc. Inst. Acoust. **27**(2), 28–35 (2005).
[52]DIN 56950-1:2012-05, "Entertainment technology—Machinery installations—Part 1: Safety requirements and inspections" (2012).
[53]D. C. Wilcox, "Reassessment of the scale-determining equation for advanced turbulence models," AIAA J. **26**(11), 1299–1310 (1988).
[54]F. R. Menter, "Two-equation eddy-viscosity turbulence models for engineering applications," AIAA J. **32**(8), 1598–1605 (1994).
[55]V. Adams and A. Askenazi, *Building Better Products with Finite Element Analysis* (OnWord Press, Florence, KY, 1999).
[56]G. H. Koopmann and J. B. Fahnline, *Designing Quiet Structures: A Sound Power Minimization Approach* (Elsevier, Amsterdam, 1997).
[57]S. Marburg and B. Nolte, *Computational Acoustics of Noise Propagation in Fluids—Finite and Boundary Element Methods* (Springer-Verlag, Berlin, 2008).
[58]J. B. Fahnline and G. H. Koopmann, "A lumped parameter model for the acoustic power output from a vibrating structure," J. Acoust. Soc. Am. **100**(6), 3539–3547 (1996).
[59]D. Fritze, S. Marburg, and H.-J. Hardtke, "Estimation of radiated sound power: A case study on common approximation methods," Acta Acust. Acust. **95**(5), 833–842 (2009).
[60]M. Klaerner, M. Wuehrl, L. Kroll, and S. Marburg, "Accuracy of vibro-acoustic computations using non-equidistant frequency spacing," Appl. Acoust. **145**, 60–68 (2019).
[61]*COMSOL Multiphysics*, v. 5.4, COMSOL AB, www.comsol.com (Last viewed 02/29/2020).